AGU PUBLICATIONS

Geochemistry, Geophysics, Geosystems

RESEARCH ARTICLE
10.1002/2014GC005683

An open source Bayesian Monte Carlo isotope mixing model with applications in Earth surface processes

Carli A. Arendt[1], Sarah M. Aciego[1], and Eric A. Hetland[1]

[1]Department of Earth and Environmental Sciences, University of Michigan, Ann Arbor, Michigan, USA

Key Points:
- Open source BMC model determines source contributions in Earth surface systems
- Effectively applied to stable and radiogenic isotope systems in various settings
- Model able to encompass end-member uncertainties and multiple isotopic systems

Supporting Information:
- Supporting Information S1
- Software S1

Correspondence to:
C. A. Arendt,
carliana@umich.edu

Citation:
Arendt, C. A., S. M. Aciego, and E. A. Hetland (2015), An open source Bayesian Monte Carlo isotope mixing model with applications in Earth surface processes, *Geochem. Geophys. Geosyst.*, *16*, 1274–1292, doi:10.1002/2014GC005683.

Received 13 DEC 2014
Accepted 19 MAR 2015
Accepted article online 27 MAR 2015
Published online 3 MAY 2015

Abstract The implementation of isotopic tracers as constraints on source contributions has become increasingly relevant to understanding Earth surface processes. Interpretation of these isotopic tracers has become more accessible with the development of Bayesian Monte Carlo (BMC) mixing models, which allow uncertainty in mixing end-members and provide methodology for systems with multicomponent mixing. This study presents an open source multiple isotope BMC mixing model that is applicable to Earth surface environments with sources exhibiting distinct end-member isotopic signatures. Our model is first applied to new $\delta^{18}O$ and δD measurements from the Athabasca Glacier, which showed expected seasonal melt evolution trends and vigorously assessed the statistical relevance of the resulting fraction estimations. To highlight the broad applicability of our model to a variety of Earth surface environments and relevant isotopic systems, we expand our model to two additional case studies: deriving melt sources from $\delta^{18}O$, δD, and ^{222}Rn measurements of Greenland Ice Sheet bulk water samples and assessing nutrient sources from ε_{Nd} and $^{87}Sr/^{86}Sr$ measurements of Hawaiian soil cores. The model produces results for the Greenland Ice Sheet and Hawaiian soil data sets that are consistent with the originally published fractional contribution estimates. The advantage of this method is that it quantifies the error induced by variability in the end-member compositions, unrealized by the models previously applied to the above case studies. Results from all three case studies demonstrate the broad applicability of this statistical BMC isotopic mixing model for estimating source contribution fractions in a variety of Earth surface systems.

1. Introduction

Both stable and radiogenic isotopes provide insight to the provenance of source material in Earth surface systems. Coupled with a Bayesian Monte Carlo (BMC) mixing model, isotopic tracers can be used to determine fractional contributions of multiple end-members to a bulk sample (i.e., water, soil, etc.). This information is crucial in understanding processes such as glacier melt evolution [*Bhatia et al*., 2011; *Cable et al*., 2011], the nutrient sources for soil development and sustainability [*Chadwick et al*., 1999], the impact of pollution on a natural system [*Barber and Wearing*, 2001], stable and radiogenic isotopes in seawater [*Pichler*, 2005; *Rickli et al*., 2010], and water usage within ecosystems [*McCluney and Sabo*, 2010; *Grupe*, 2014].

Implementing Bayesian estimation techniques allows for the representation of spatiotemporal processes, incorporation of uncertainties, and extrapolation of input source magnitudes, and accounts for prior information and assumptions [*Soulsby et al*., 2003; *Wikle*, 2003; *Singh and Bengtsson*, 2005; *Moore and Semmens*, 2008]. The goal of this study is to develop and provide the Earth science community with an open source, statistically robust, BMC isotope mixing model that can be applied to both stable and radiogenic isotopic systems in a variety of Earth surface processes. The model is executed in a straightforward Matlab script, which is easy to implement and modify by researchers with minimal programming experience.

The advantage of the isotope statistical model presented in this study is that model inputs are straightforward, requiring only an Earth system with unique end-member isotopic signatures [*Theakstone*, 2003] and measurements of a sample's isotopic composition. Another benefit of this model is that it incorporates uncertainty in end-member isotopic compositions and provides an uncertainty estimation of the fractional contributions. Stable isotopes $\delta^{18}O$ and δD have commonly been used to determine contributing water sources and relative proportions of these sources to a system. Radiogenic isotopes ϵ_{Nd}, $^{87}Sr/^{86}Sr$, and ϵ_{Hf} have frequently been applied to terrestrial and oceanic settings to identify the provenance of and inputs to regolith, soils, and water masses.

Earth surface $\delta^{18}O$ and δD samples are easy to collect, require no special sampling equipment or need for low-blank, metal-free cleanliness, and are time insensitive if the collection vials are sealed properly. Radiogenic Earth surface ϵ_{Nd}, $^{87}Sr/^{86}Sr$, and ϵ_{Hf} samples require additional precaution in their collection and analyses, but are gaining accessibility as the application of these isotopes is expanding. Both stable and radiogenic isotope systems in these Earth surface environments can be addressed by the model presented in this study.

For this work, we developed a BMC mixing model and applied it to a new set of $\delta^{18}O$ and δD measurements of bulk meltwater collected from the Athabasca Glacier during the summer of 2011. The aim of this study was not to expose an unknown seasonal progression, but to corroborate the effectiveness of our model by comparing our resulting fractional contribution estimations to expected seasonal melt source contribution trends. The application of the model to this data set allowed us to quantify the actual proportion and volume of water coming from each end-member source, which holds importance for relative contributions of snowmelt versus ice melt in the context of water storage and hydrologic use. We include a thorough description of the field site, sampling methods, analytical techniques, seasonal trend analysis, and statistical relevance of the calculated end-member fractional contributions for the Athabasca Glacier.

We apply the same type of multicomponent linear mixing model to two additional case studies, one in Greenland and the other in Hawaii, which have already been subjected to simple isotope mixing models, to test the applicability and accuracy of our model. Lengthy descriptions of sampling, analysis, and discussion of implications of results are not included for the Greenland Ice Sheet nor the Hawaiian soil case studies, as the implications from these data sets and estimated fractional contributions have already been addressed in previous publications [*Kennedy et al*., 1998; *Chadwick et al*., 1999; *Kurtz et al*., 2001; *Chadwick et al*., 2009; *Bhatia et al*., 2011], and are used only to assess the applicability to additional isotopic and Earth surface systems.

1.1. Bayesian Mixing Model

Initially motivated by *Ogle et al*. [2004] and *Cable et al*. [2011], we developed a Bayesian Monte Carlo (BMC) estimation strategy, to solve for fractional contributions of end-member compositions from isotopic measurements. The BMC strategy is such that samples of a prior probability density function (PDF) are retained or rejected in proportion to data likelihood, resulting in samples of a posterior PDF [e.g., *Mosegaard and Tarantola*, 1995]. Bayes' theorem as applied to our estimation of fractional contributions is

$$p(f_i) \propto p'(f_i \ \& \ I_i)\, L(o_j | f_i \ \& \ I_i), \tag{1}$$

where f_i are the fractional contributions (i.e., the unknown model), o_j are the isotopic measurements, I_i are the isotopic composition of the end-member components, $p(f_i)$ and $p'(f_i \& I_i)$ are the prior and posterior PDFs, respectively, and $L(o_j | f_i \ \& \ I_i)$ is a data likelihood function. Bayesian estimation narrows the given prior PDF to a posterior PDF by testing the statistical likelihood of predicted isotopic values against the observations [e.g., *Mosegaard and Tarantola*, 1995].

The prior PDF includes both the isotopic compositions of the end-member components and constraints on the fractional contributions of the end-member components. Rather than assuming that the isotopic composition of the end-members are precisely known, we include variances of the end-member compositions in the prior PDF, where the variances can account for either uncertainty in the compositions or natural variability in the end-member components. *Cable et al*. [2011] and *Parnell et al*. [2013] assumed a specialized covariance model of the uncertainties assuming that the isotopic compositions of each end-member directly influence the mass fractionation of the other end-members. We have no evidence to support this complexity of the end-member covariance in the case studies presented here. Hence, we follow a simpler approach in which we assume that the uncertainties of the isotopic compositions of the end-members are uncorrelated and that the end-member compositions are normally distributed with standard deviation given by the measurement uncertainties: although use of other PDFs, either analytic or empirical, can be included.

The priors of the fractional contributions can include detailed prior knowledge and assumptions of the fractional contributions or, can consist of more simple priors in which the sum of all fractional contributions is equal to one. The applications presented here use the latter. Specifically, all the applications presented here

assume that there are only three possible contribution sources (see below for discussion of additional sources), and in this case the constraint is

$$f_a + f_b + f_c = 1, \tag{2}$$

where f_a, f_b, and f_c are the fractional contributions of the three sources. Additional end-members may be added so long as there are an equal number of constraints and/or system equations, which are given by the number of isotopic species considered. Other than the constraints in equation (2), we assume all combination of $0 \geq f_i \leq 1$ are equally likely.

Additional constraints may be added to the prior without the addition of end-members to increase the certainty of the fraction predictions. Constraints may be incorporated to narrow the possible range of values within which a mass fraction must lie. For time series data sets, a potential constraint could be the expected likelihood of certain estimations at different time periods. Likewise, expected temporal variations of the end-member isotopic composition could also be incorporated into the prior. For example, temporal constraints could account for variation of fractionation of δ^{18}O during snowmelt, where the variance on the end-member δ^{18}O may be smaller during time periods with minimal snowmelt (e.g., late summer, fall) and larger during time periods with maximum snowmelt (e.g., spring, early summer). In the applications we present, we make no assumption about how the fractional contributions vary through time and estimate the posterior PDFs independently at each time for which the data are available.

We assume purely Gaussian (normal) and uncorrelated uncertainties on the measured isotopic compositions. The data likelihood function is then given as

$$L(o_j | f_i \ \& \ I_i) \propto \prod_j \exp\left[\frac{(o_j^p - o_j)^2}{2\sigma_j^2}\right], \tag{3}$$

where σ_j are the uncertainties on the isotopic measurements and o_j^p are the isotopic values predicted by a test model of f_i and realization of I_i. To compute the predicted isotopic values, we use a standard linear mixing model [*Sharp et al*., 1995; *Ogle et al*., 2004; *Moore and Semmens*, 2008; *Bhatia et al*., 2011; *Cable et al*., 2011; *Parnell et al*., 2013], which is discussed in detail for each case study below. An additional complication in the mixing relationship arises when the values of the isotopic complications of the three source end-members are not precisely known, and the degree to which they are known is not explicitly characterized [*Theakstone*, 2003; *Moore and Semmens*, 2008; *Parnell et al*., 2010]. We deal with this complication by including variability of the end-member compositions in the prior, as discussed above. The consideration of more isotopic tracers with distinct end-member compositions would in general result in lower final uncertainties in the final posteriors, which is discussed explicitly in Case Study 2 below.

We use a straightforward Monte Carlo sampling scheme, where randomly chosen samples of the prior are retained as samples of the posterior proportional to the likelihood based on the mistift between predictions and data. The samples of the prior represent random realizations of end-member contributions and fractions of contributing components. The retained samples are then samples of the posterior PDF and represent fractional contributions of the end-members. Rejection and acceptance of the prior samples is relative to the most likely model. For example, prior samples are always accepted if the relative likelihood is one (i.e., the most likely estimate), accepted half of the time with 50% probability if the relative likelihood is 0.5, and never accepted if the relative likelihood is zero.

The Monte Carlo sampling strategy we use is equivalent to a uniform random walk in which no transitional properties are needed [e.g., *Mosegaard and Tarantola*, 1995]. Our approach is in contrast to the Markov Chain Monte Carlo (MCMC) Bayesian approach used by *Cable et al*. [2011] where the selection of prior samples is based on the likelihood of a proposed sample relative to the likelihood of the previous sample tested [e.g., *Mosegaard and Tarantola*, 1995]. While our uniform BMC is less computationally efficient than a MCMC approach, the linear mixing system is computationally trivial and sufficient posterior samples can be determined on an average desktop computer in a tractable time frame (roughly 20 min to several hours on a standard desktop computer, depending on sample size).

For each stock measurement, we tested approximately 10^7 prior samples and accepted those as posterior samples in proportion to the relative likelihood of their associated prediction. In each run we present here,

$1-8\times10^4$ samples were found to be statistically likely relative to the most likely estimate for each stock sample. The density in the fractional contribution space of the accepted posterior samples reflects the statistics of the estimated fractional contributions and is statistically consistent with the measurements. We calculate mean values, standard deviations, and covariance of the posterior samples (i.e., fractions of the source contributions) for each stock sample. The normal statistical moments characterize the posteriors well, although it is important to bear in mind that the posteriors are bound by the constraints of the solutions (i.e., all fractional contributions are ≥ 0 and must sum to 1), and thus are non-Gaussian. Covariance values reflect how dependent the fractional contribution of each individual end-member is on the projected fractional contribution of the other end-members.

2. Case Studies

2.1. Case Study 1: Glacial Meltwater Fractions Based on $\delta^{18}O$ and δD From the Athabasca Glacier

The Athabasca Glacier is one of eight outlet glaciers draining the Columbia Icefield, a 325 km^2 ice plateau (Figure 1). The Columbia Icefield straddles the continental divide in the Canadian Rocky Mountains, lying at the north end of Banff National Park and the south end of Jasper National Park in Alberta, Canada. The Columbia Icefield is approximately 1900 m at the lowest elevation and 3400 m at the highest point, Snow Dome. The Athabasca Glacier connects to the Columbia Icefield at approximately 2700 m and extends down to 2030 m at its terminus. Melt from the Columbia Icefield drains into three major oceans, including the Arctic, Pacific, and Atlantic oceans, but is located over 2000 km from the nearest ocean [*Butler*, 1980; *Brugmann and Demuth*, 1994; *Hart*, 2006].

Local climate in the Columbia Icefield region has remained relatively consistent throughout the past half century [*Letreguilly*, 1988; *Canada National Climate Archive*, 2013] with no abrupt changes, although the local mean annual temperature has been gradually increasing [*Canada National Climate Archive*, 2013]. In the past decade, average local winter temperatures ranged from -15 to -19°C, summer temperatures ranged from $+16$ to $+20^\circ$C, and annual temperatures averaged $+1^\circ$C [*Shea and Marshall*, 2007; *Canada National Climate Archive*, 2013]. Total annual precipitation for the region has ranged from 395 to 475 mm in the past decade, with the majority coming from snowfall (~65–90%) [*Shea and Marshall*, 2007; *Canada National Climate Archive*, 2013]. The balance between mass gain through annual precipitation and mass loss through ablation, primarily melting, has trended toward mass loss since the Little Ice Age, and the Athabasca Glacier retreats several meters annually [*Hart*, 2006].

Meltwater from the Columbia Icefield recharges the local confined aquifer, and subglacial melting is responsible for the development of a karst system between the Castleguard and Saskatchewan glaciers [*Ford et al.*, 1983; *Smart*, 1983], which are outlet glaciers to the south of the Athabasca Glacier. The lithology beneath the Athabasca Glacier consists of Middle Cambrian limestone and carbonic shale, which allow for karst formation [*Hart*, 2006]. Discharge from the aquifer occurs via large springs between 1500 and 1900 m in elevation throughout the region [*Ford et al.*, 1983], and there is a proximal spring to the Athabasca Glacier approximately 130 m lower in elevation than the terminus (Figure 1). There is an absence of groundwater input to the subglacial environment because the aquifer is confined and located at lower elevation than the terminus of the Athabasca Glacier. Thus, snowmelt, ice melt, and summer precipitation are the primary contributions to the water discharge from the Athabasca Glacier terminus.

Because the Athabasca Glacier is an outlet glacier of a larger ice body, the mass balance of the Columbia Icefield directly impacts the mass balance of the Athabasca Glacier. The accumulation area, the Columbia Icefield plateau, accumulates summer and winter snow, has little surface melt, and produces the blue ice that is ultimately exposed in the ablation zones of its outlet glaciers, including the Athabasca Glacier. Summer ablation from the outlet glaciers will include both winter snowpack deposited on the glacier surface and blue ice from the Columbia Icefield that is a combination of both summer and winter deposition.

2.1.1. Sample Collection and In Situ Measurements

Water samples were collected from the main outlet channel 10 m downstream from the Athabasca Glacier terminus (located 2030 m above sea level at N52°12.54 and W117°14.29). In situ measurements took place every morning in May and July 2011 alongside samples that were being collected for a corresponding study of Athabasca Glacier subglacial water residence time (C. A. Arendt et al., Uranium-series isotopes confirm prolonged residence time of subglacial water, submitted to *Earth Planetary Science Letter*, 2015). Samples

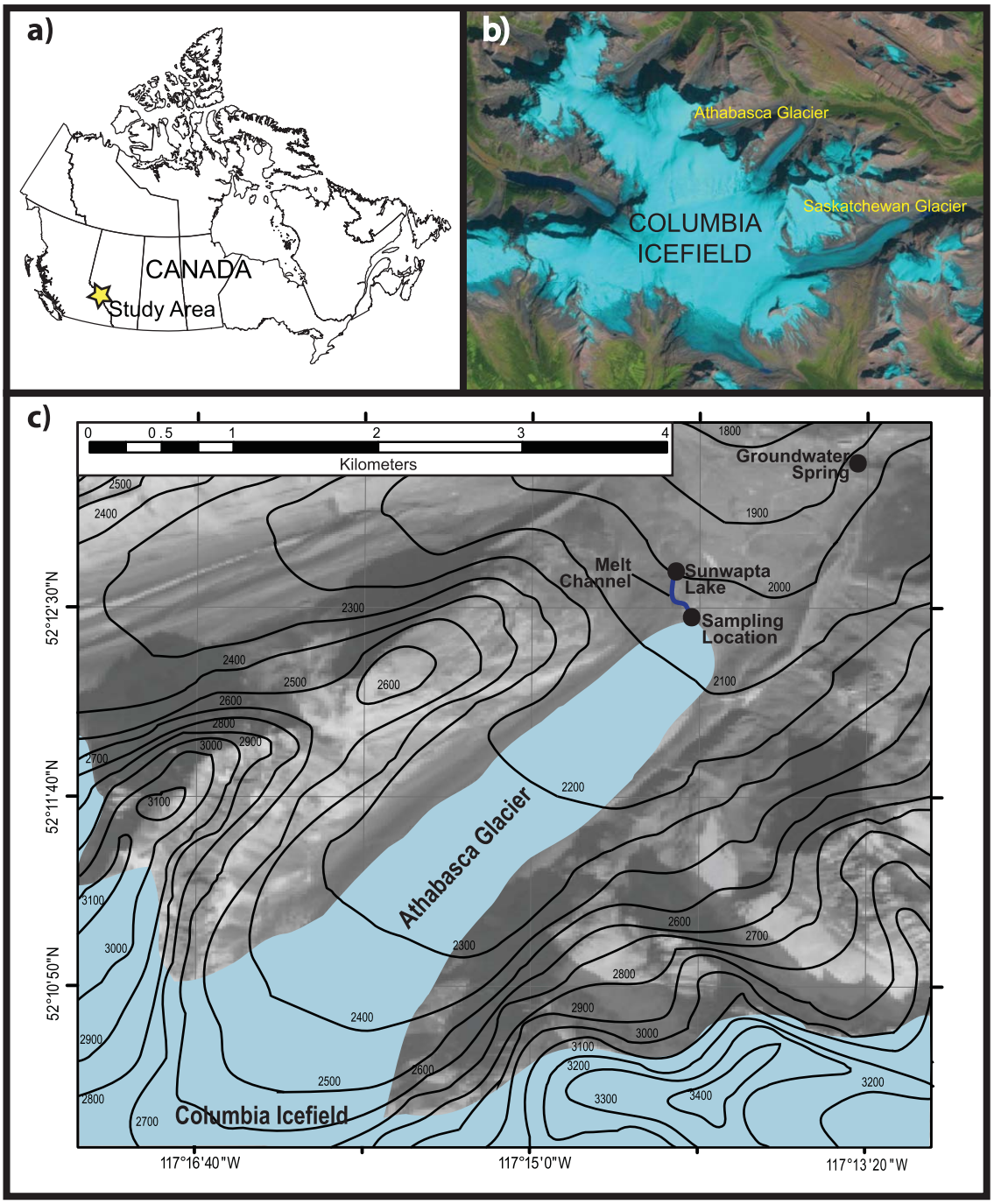

Figure 1. Location map of sampling site (a) Athabasca Glacier (yellow star) is located in Jasper National Park, Alberta, Canada. (b) The Athabasca Glacier is a prominent lobe coming off of the Columbia Icefield, situated in the Canadian Rockies. (c) Sampling site at the terminus of the Athabasca Glacier is indicated by a black circle, at N52°12.54, W117°14.29. Sampling took place at the main meltwater channel, within 20 m of the ice terminus of the Athabasca Glacier. A melt channel connects our sampling site to Lake Sunwapta (black circle), located approximately 0.25 km from the terminus of the Athabasca Glacier. A black circle approximately 1.5 km from the terminus of the Athabasca Glacier and over 150 m lower in elevation than our sampling location denotes a local groundwater spring. Map is composed of a Digital Elevation Model (DEM), which shows elevation contour lines at 100 m, ranging from lowest elevation of 1800 m to the highest elevation of 3400 m, overlain onto 12 Systeme Pour l'Observation de la Terre, SPOT.

were collected at the same time daily (in the morning) for consistency and to avoid variations in bulk melt sample composition due to daily fluctuations. The data set consisted of samples collected in May and July, but not June because of the time and resource intensiveness required for obtaining a suite of time series samples. Thus, the collection season was scheduled to align with the hydrologically important time periods,

Table 1. Isotopic End-Member Values and Number of Samples (n) Collected for the Athabasca Glacier Case Study That Were Either Directly Measured or Referenced From Regional Databases [*Canada National Climate Archive*, 2013] As Described in Case Study 1

End-Member	$\delta^{18}O$	$\sigma\delta^{18}O$	δD	$\sigma\delta D$	n
Ice melt	−20.0	0.5	−140.0	2.0	4
Snowmelt	−25.5	0.7	−205.0	4.0	4
Summer precipitation	−13.0	2.0	−104.0	10.0	n/a

including onset and peak of melt. Similar strategies have been employed in previous studies [e.g., *Bhatia et al*., 2011]. Samples collected for oxygen and hydrogen isotopes were collected onsite directly into Kimble™ 20 mL glass screw-thread scintillation vials (No. 7451620) with cone caps. Vials were filled to the top to minimize atmospheric head space and sealed tightly until measurement.

Daily discharge measurements were taken concurrently, at the same location and time that the water samples were collected. Manual measurements of discharge were acquired using an Acoustic Doppler Velocimeter, or ADV, Flow-tracker. A measuring tape was set across the width of the channel, perpendicular to water flow. The ADV Flowtracker's sensor was submerged at the edge of the channel parallel to water flow and calibrated prior to measurement. Following calibration, the ADV Flowtracker measured velocity and water depth at one-foot increments spanning the width of the main discharge channel at the terminus of the glacier. Velocity and water depth measurements across the channel allowed the calculation of discharge, using the standard 0.6 rule [*Morlock et al*., 2002] (see supporting information, Table S1), and subsequently converted from cubic feet per second to cubic meters per second.

The stable isotope compositions of ice and snow samples were collected from the terminus (∼2030–2050 m ASL) of the Athabasca Glacier (Table 1). End-member samples of snow were collected at the beginning and end of the field season and averaged. End-member samples of ice were collected across a horizontal transect of the glacier to encompass a range of ice ages and averaged. Precipitation values were not directly collected as the directionality and timing of precipitation events made the collection of an adequate sample volume impossible. Thus, 2011 summer precipitation $\delta^{18}O$ and δD values were compiled from three regional weather stations for the years 2010–2011 including *Athabasca 1* (N54°43.20, W113°17.17), *Athabasca AGCM* (N54°38.05, W113°22.55), and *Athabasca LO* (N52°25.00, W117°47.00) [*Shea and Marshall*, 2007; *Canada National Climate Archive*, 2013]. Precipitation isotopic values were averaged and used as the representative precipitation end-member. These three distinct isotopic signatures for contributing water masses to the Athabasca Glacier subglacial discharge are defined in Table 1. The ranges in end-member isotopic measurements, both directly measured and taken from literature, are accounted for as the standard deviation of each end-member value given (Table 1).

2.1.2. Mass Spectrometry

Water stable isotope measurements were performed at the University of Michigan Stable Isotope Laboratory. Deuterium measurements were made using a Finnigan H-Device coupled to a dual inlet gas source Thermo Finnigan Delta V Plus mass spectrometer. The analysis process entailed use of an A CTC Analytics Pal Autosampler to inject 1 mL of water per sample into a chromium reactor set at 800°C, where the sample reacts for approximately 2 min. Next, the samples were equilibrated in the dual inlet for 1 min (allowing the H_2O and CO_2 in the system to reach isotopic equilibrium) and run at 8 V against a reference gas of known composition [*Socki et al*., 1992]. The samples were run in duplicate to account for memory effects and bracketed against known standards (VSMOW/VSLAP, in-house standards) to ensure accuracy in the machine's measurements. Sample measurements were then normalized relative to the VSMOW/VSLAP scale and expressed relative to VSMOW. Accuracy and precision is better than $\pm 1‰$ on replicate analyses, and analytical error on standards over time is better than $\pm 1.3‰$.

Oxygen isotopes ($^{18}O/^{16}O$) were measured by continuous flow on a Thermo Finnigan Gas Bench II coupled to the inlet of a Thermo Finnigan Delta V Plus mass spectrometer. The analysis process entailed use of an A CTC Analytics Pal Autosampler to inject 0.5 mL of water per sample into a preevacuated Labco exetainer. Next, the samples were loaded into the Finnigan Gas Bench II sample tray. The A CTC Analytics Pal Autosampler was used to flush the samples with 0.3% CO_2 in a helium (He) mixture for 8 min. The samples were then allowed to equilibrate over a 2 day period at 30°C. Pure He (UHP grade) was then used to flush each sample for 8 min. The sample gas was then transported via helium flow, cleaned of any remaining water

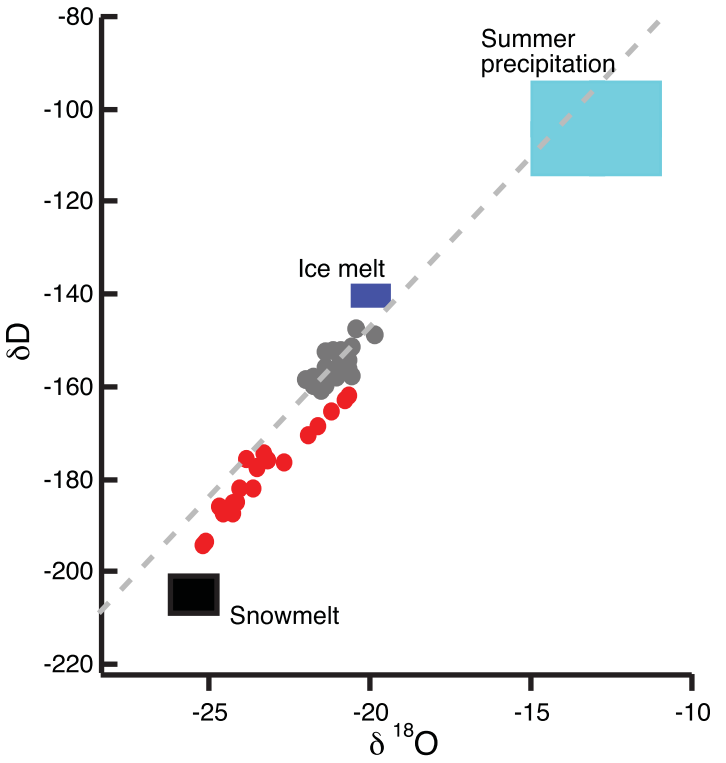

Figure 2. Dual isotope plot of $\delta^{18}O$ and δD values of Athabasca Glacier bulk water samples for May (gray) and July (red) 2011 in comparison to the Local Meteoric Water Line for Canada [*Clark and Fritz*, 1997]. Rectangles represent the mean isotopic end-member values and variation in end-member values for snowmelt, ice melt, and summer precipitation as described in the text and in Table 1.

with the Gas Bench water traps, and pushed through a GC column set at 70°C. The CO_2 was then admitted through a capillary to the inlet of the mass spectrometer where multiple sample peaks were measured against the CO_2 reference gas peaks. The data were normalized and reported relative to the VSMOW/VSLAP scale. Accuracy and precision for these samples is $\pm 0.1‰$.

The oxygen and hydrogen isotopic composition of water samples and corresponding discharge measurements from the Athabasca Glacier are summarized in Table S1.

2.1.3. Oxygen and Hydrogen Isotopic Composition of Glacial Meltwater

The stable isotopes of the bulk discharge water samples from the primary discharge channel at the Athabasca Glacier show distinct changes through the onset of summer melting in May and peak melt in July (Table S1). At the initial onset of melt our $\delta^{18}O$ and δD data become increasingly depleted only to show a reversal in trend in the second week of May, where $\delta^{18}O$ and δD become increasingly enriched in lighter isotopes for the remainder of the month. Samples from July show less enriched $\delta^{18}O$ and δD values, comparable to those samples from the very beginning of May, with no obvious temporal trends and little variation.

Results are presented in dual isotope space along with the Local Meteoric Water Line (LMWL) [*Clark and Fritz*, 1997] for Canada (Figure 2). When plotted in this manner, our $\delta^{18}O$ and δD measurements follow the expected relationship of waters in dual isotope space [*Craig*, 1961]. All meltwater samples exhibit positive deuterium excess values (d-excess $= \delta D - 7.75 \times \delta^{18}O$, where 7.75 is the slope of the LMWL). Samples from early May show the smallest deuterium excess (less than $1.0‰$), with values trending toward more positive values through May and into July (between 3 and $12‰$).

The combination of low mean annual temperatures, high elevation, and distance from precipitation source drives depletion in the stable isotopes of water, $\delta^{18}O$ and δD, via Rayleigh fractionation [*Dansgaard*, 1964; *Aizen et al*., 2005; *Cooper*, 1998; *Petit et al*., 1999; *Moore and Semmens*, 2008; *Singh*, 2013]. In addition, there is a significant seasonality to the depletion, with winter snow producing the most negative isotopic compositions. Thus, $\delta^{18}O$ and δD values of ice are medians between summer and winter snowpack $\delta^{18}O$ and δD values [*Aizen et al*., 2005; *Canada National Climate Archive*, 2013].

2.1.4. Fractional Contributions to Meltwater Discharge

We assume that the Athabasca Glacier system has three possible contribution sources: snowmelt, ice melt, and summer precipitation. Thus, the sum of the fraction from snowmelt (f_s), fraction of ice melt, (f_i), and fraction from summer precipitation/rain (f_r) is constrained to equal 1

$$f_s + f_i + f_r = 1. \quad (4)$$

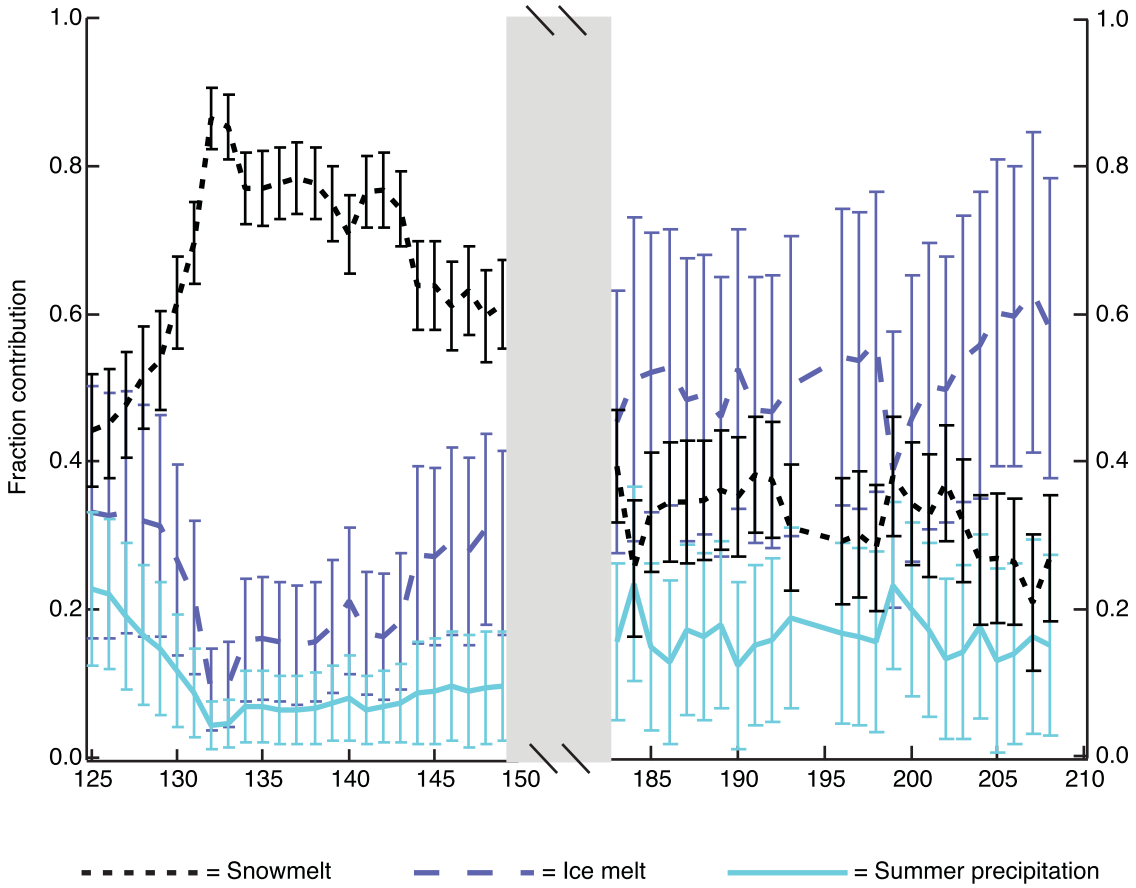

Figure 3. Time series graph of the best fit calculated f_s, f_i, and f_r to the main discharge channel of the Athabasca Glacier in May and July 2011. Sampling days where precipitation was observed in the field are presented in Table S1.

The likelihood of a model prediction was calculated using

$$L \propto \exp\left[\frac{\left(\delta^{18}O_p - \delta^{18}O_o\right)^2}{2\sigma^2_{\delta^{18}O}}\right] \cdot \exp\left[\frac{\left(\delta D_p - \delta D_o\right)^2}{2\sigma^2_{\delta D}}\right], \quad (5)$$

where $\delta^{18}O_p$ and $\delta^{18}O_o$ are the predicted and observed measurements of $\delta^{18}O$, respectively, $\sigma_{\delta^{18}O}$ is the measurement uncertainty, and likewise for δD.

Fractional contributions f_i, f_s, and f_r were estimated from the bulk water for each day that a sample was collected and the isotopic composition measured. These sample day fractional contributions at the Athabasca Glacier are summarized in the supporting information Table S2. As described above, we characterize the posteriors (or uncertainty of PDFs after incorporating additional constraints) by the averages, variances, and covariances calculated. In Figure 3, we show the average estimated fractional contributions for each DOY and in Figure 4 we show the 67% credible ellipses of multivariate Gaussian PDFs describing the posteriors. We chose to 67% (mean value $\pm 2\sigma$) instead of 95% (mean value $\pm 1\sigma$) credible intervals to optimize the clarity of the plots. In supporting information Figure S1, we compare the 67% ellipse to the full posterior corresponding to the 200th day of 2011, which is a representative posterior of all of the days.

Model results show that in May the dominant contributor to the water volume at the main discharge outlet varied temporally. Initially, the base flow comprised approximately equal parts f_i, f_s, and f_r, but shifted within several days to primarily f_s (Figure 3). The range of fractional contributions for the end-members in May was 0.44–0.86 (f_s), 0.09–0.33 (f_i), and 0.04–0.23 (f_r). In July the contribution fractions had evolved so that f_i was

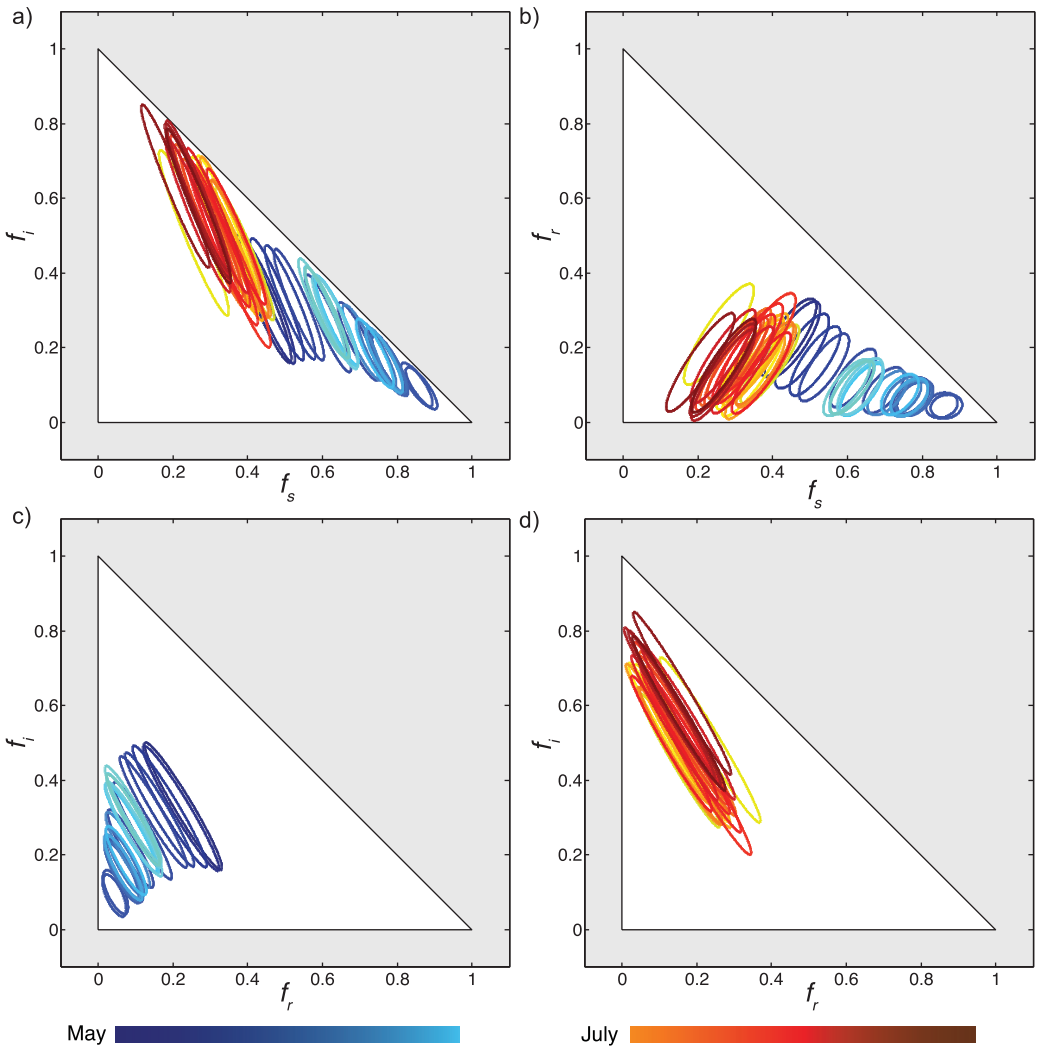

Figure 4. The 67% credible ellipses (mean $\pm 2\sigma$) of multivariate Gaussian PDFs fit to the posteriors of estimated fractional contributions for May and July 2011. Credible ellipses depict the mean, standard deviations, and covariance of the posteriors (see Figure S1 for a graphical comparison of the 67% ellipse and the full posterior corresponding to the 200th day of 2011). Color of the ellipses corresponds to the sample day, with blue to cyan corresponding to days in May and yellow to red corresponding to days in July, depicting early to late in each respective month.

the main contributor, followed by f_s and f_r. The range of fractional contributions for the end-members in July was 0.44–0.63 (f_i), 0.08–39 (f_s), and 0.12–0.23 (f_r). Throughout the duration of our field season, f_r was always the smallest mass contributor, ranging consistently between 0.04 and 0.23 in both May and July.

The estimated fractional contributions are more uncertain in July than in May, in particular the uncertainty in f_i is larger in July than in May (Figure 4). f_i is negatively correlated to both f_s and f_r, with the correlations slightly stronger in July than in May (Figure 4). In contrast, covariances between f_s and f_r generally indicate moderate positive correlations (Figure 4b).

For all end-member relationships, the errors in the covariance of fractional contribution in July are significantly larger than the errors in the covariance of fractional contribution in May (Figure 4). The smaller errors in May are likely due to the fact that snow dominated as the most available melt source and that precipitation was limited; thus, the system was primarily two-component mixing and the isotopic composition was clearly closer to an end-member composition. In July, f_i became the dominant contributor and the composition of the bulk mixture had almost equivalent source components; thus, small variations in the relative contributions have large uncertainty in our BMC model. Not surprisingly, there is significant covariance between f_s and f_i because they are the two most abundant end-members, are dominantly driven by air temperature, and provide the largest volumetric input to the main outlet channel.

2.1.5. Snowmelt Versus Ice Melt Discharge

The prominent seasonal shift in the dominant source of the discharged water at the terminus of the Athabasca Glacier signifies a change in the volume of snow and ice available for melt contributions. In May the length of the Athabasca Glacier was blanketed by snow cover, which insulated the underlying surface ice. Thus, the primary ice melt in May is derived from basal ice. In July the snow extent had retreated up-glacier by approximately 1 km, exhausting the available snow supply and exposing glacial ice to the atmosphere and solar radiation.

We calculated the glacial discharge originating from each source using daily in situ discharge measurements and the model calculated fractional contributions. While the fraction input from each melt source shifts drastically from May to July, in the context of the water volume initiating from f_i, f_s, and f_r, the difference between melt generated, or water volume being discharged from the Athabasca Glacier, shows that melt contribution volumes were far more significant in July than in May (Table S1). Although we assume the fractional contributions were approximately constant throughout the day, we note that discharge measurements were taken in the morning and discharge volumes likely increased with increasing temperature throughout the course of a day. Observations of precipitation at our sampling site (Table S1) are in agreement with the major f_r spikes produced by our model (Figure 3), confirming that our model is consistent with the physical system. DOY 199 in (Figure 3) stands out in that the f_i decreases significantly while the f_s and f_r increase. The spike in f_r is corroborated by our in-field observations of precipitation on that day (Table S1) and an increase in f_s is likely due to increased surface melt caused by precipitation. Hence, the ice melt volume may not have decreased but the overall f_i must decrease to encompass the sudden increase in precipitation and f_s.

The prominence of f_i in July indicates that the Athabasca Glacier drainage basin would have a high base flow water discharge available even in the absence of snowmelt. Our calculations are in agreement with the general observation that glacial watersheds are tremendous natural reservoirs that can store and produce freshwater over millennial time scales [*Verbunt et al*., 2003; *Barnett et al*., 2005; *Singh and Bengtsson*, 2005; *Thayyen et al*., 2007; *Kehrwald et al*., 2008; *Fortner et al*., 2009] whereas snow-only watersheds are typically depleted annually [*Verbunt et al*., 2003; *Singh and Bengtsson*, 2005; *Thayyen et al*., 2007; *Liu et al*., 2008; *Stewart*, 2009]. Glacial melt from the Columbia Icefield and the Athabasca Glacier has helped maintain the water balance of many rivers and lakes in Alberta [*Ford et al*., 1983; *Smart*, 1983; *Falcone*, 2007]. However, if the Athabasca Glacier continues to retreat, it has the potential to become a snow-dominated watershed, which could reduce the water supply by a half and negatively impact the human and biotic communities that rely on a certain base flow water discharge [*Barnett et al*., 2005].

2.1.6. Potential Caveats

Previous studies have suggested that the δ^{18}O and δD composition of snowpack can fractionate through time due to equilibrium isotopic exchange between the snowmelt and residual snowpack; observations from the Sierra Nevada snowpack indicate a 3–4‰ shift in the δ^{18}O of snowmelt per year [*Taylor et al*., 2001; *Unnikrishna*, 2002]. However, the assigned standard deviations (Table 1) encompass a significant portion of this shift and the increase to δ^{18}O values of $-23‰$ is likely not due to complete melting of the snowpack given that we observed more than 1 m of snow on top of the glacier at the end of May. The difference between the minimum δ^{18}O values in May and the δ^{18}O values in the beginning of July is $\sim$4‰, which lies within the range of expected fractionation [*Cooper*, 1998] (Table S1). Therefore, to the first order, our model is an accurate representation of source partitioning fluxes from a glacial watershed.

Our model also does not differentiate between contributions of δ^{18}O and δD at the surface, exposed to evaporation to the atmosphere, and those in the basal environment, exposed to winter refreezing. These processes generally only change the deuterium excess [*Craig*, 1961; *Hooper and Shoemaker*, 1986; *Gat*, 1996], whereas changes in the primary isotopic compositions are within the uncertainties of the end-member values we assumed. Variations in deuterium excess in this glacial environment are likely driven by refreezing of subglacial ice [*Souchez et al*., 1983; *Souchez*, 1984; *Hubbard et al*., 1995; *Souchez*, 2000], but modeling this process is beyond the scope of the work presented in this paper.

2.2. Case Study 2: Quantifying Surface Versus Basal Glacial Melt Using δ^{18}O and ^{222}Rn From the Greenland Ice Sheet

The Greenland Ice Sheet (GrIS) is the largest ice mass in the Northern Hemisphere, and represents a potentially massive source of meltwater to the world's oceans. Placing constraints on the proportion of different

Table 2. Isotopic End-Member Values From Bhatia et al. [2011] GrIS Samples[a]

End-Member	$\delta^{18}O$	$\sigma\delta^{18}O$	δD	$\sigma\delta D$	^{222}Rn	$\sigma^{222}Rn$
Surface snow	−12.3	1.2	−89.9	9.0	0.0	0.0
Glacial ice	−28.2	2.8	−216.1	21.6	0.0	0.0
Delayed flow waters	−29.6	3.0	−222.7	22.3	209.5	52.4

[a]Uncertainties were assigned at 10% for $\delta^{18}O$ and δD and 25% for ^{222}Rn for this case study.

water sources and how they evolve seasonally would further our understanding of melt dynamics, and thus the GrIS's likely response to global warming. In a study published in 2011, Bhatia et al. collected bulk meltwater from a small land-terminating outlet glacier on the Southwest margin of the GrIS, approximately 125 km south of the well-studied Jakobshavn Isbrae. Samples representing bulk subglacial discharge were collected during the peak melt of 2008 from the primary outflow directly at the margin of the outlet glacier. End-member samples of surface snow, glacial ice, and delayed flow (described below) were collected from surface snow and surface melt ponds, glacial ice samples, and a proglacial stream, respectively. The samples were analyzed for $\delta^{18}O$ and δD in a laboratory and ^{222}Rn was measured in situ. These isotopes were ultimately incorporated into a simple linear mixing model based on invariant end-member composition [*Bhatia et al.*, 2011].

The distinct isotopic $\delta^{18}O$ and δD signatures of the end-members in this case study allow for the assessment of bulk water isotopic composition to ascertain fractional contributions from end-members of snow and ice, similar to the methods used in the Athabasca Glacier case study. However, the third isotope used in this case study, ^{222}Rn, is applied primarily to constrain the fractional contribution from the delayed flow component, derived from water melting in the subglacial environment, as both surface snow and glacial ice melted in contact with the atmosphere do not contain detectable amounts of ^{222}Rn. End-member $\delta^{18}O$, δD, and ^{222}Rn values can be found in Table 2. The bulk composition water $\delta^{18}O$ and ^{222}Rn measurements are plotted with the source end-member $\delta^{18}O$ and ^{222}Rn measurements in Figure 5. In this case study we assess the uncertainties associated with fractional contribution estimates using both a two isotope system model and a three isotope system model.

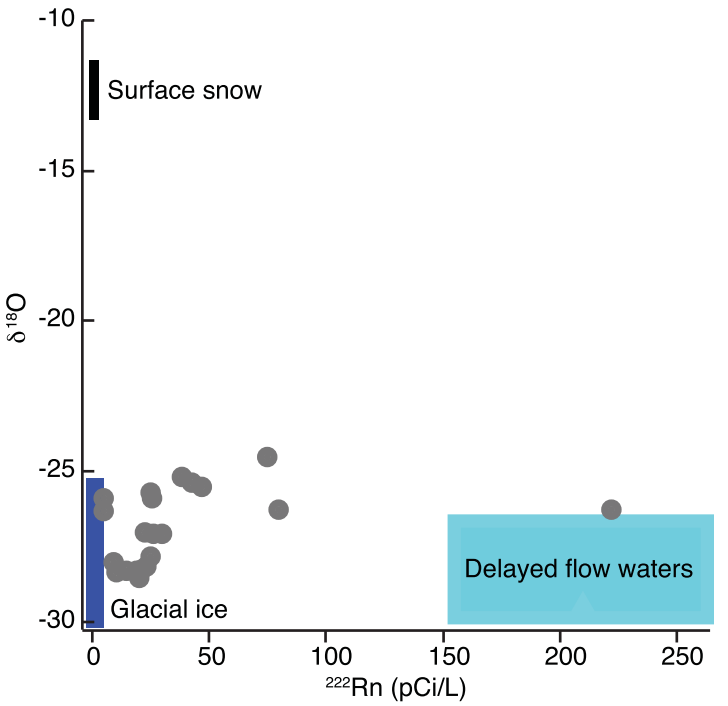

Figure 5. Dual isotope plot of $\delta^{18}O$ and ^{222}Rn values of Greenland Ice Sheet bulk water samples for May and July 2008. Rectangles represent the mean isotopic end-member values and variation in end-member values for surface snow, glacier ice, and delayed flow waters, taken from *Bhatia et al.* [2011]. End-member isotopic compositions and uncertainties can be found in Table 2.

2.2.1. Fractional Contributions to Greenland Ice Sheet Bulk Meltwater

In the original study, *Bhatia et al.* [2011] found that the main source contributor to the bulk meltwater samples collected from the GrIS during the onset of melt in the summer of 2008 was delayed flow waters, which composed 0.10–0.70 fractional contribution in May and decreased to 0.04–0.18 in July. In contrast, the glacial ice fractional contributions increased from 0.02–0.70 in May to 0.80 and 0.95 in July, and the surface snow contribution stayed consistently between 0.15 and 0.35 in May and decreased to less than 0.08 in July.

Bhatia et al. [2011] employed a linear isotope mixing model with invariant end-member

compositions, using $\delta^{18}O$, δD, and ^{222}Rn, to estimate fractional contributions of surface snow, glacial ice, and delayed flow waters to the GrIS meltwater. To evaluate these estimates, and associated uncertainties, we input their $\delta^{18}O$, δD, and ^{222}Rn into our BMC model. We also explicitly test the decrease in uncertainty associated with increasing the number of constraints by comparing the model with two isotope systems ($\delta^{18}O$-^{222}Rn) and three isotope systems ($\delta^{18}O$-δD-^{222}Rn). We compare the resulting fractional contribution estimates to the results of *Bhatia et al.* [2011].

In the application of our model to this case study, we assume that these GrIS samples have three possible contribution sources: surface snow, glacial ice, and delayed flow waters. Thus, the sum of the fraction from surface snow (f_{ss}), fraction from glacial ice (f_g), and fraction from delayed flow waters (f_d) is constrained to equal 1

$$f_{ss}+f_g+f_d=1. \tag{6}$$

The likelihood of a model prediction was calculated using

$$L \propto \exp\left[\frac{\left(\delta^{18}O_p-\delta^{18}O_o\right)^2}{2\sigma^2_{\delta^{18}O}}\right]\cdot\exp\left[\frac{\left(^{222}Rn_p-^{222}Rn_o\right)^2}{2\sigma^2_{^{222}Rn}}\right], \tag{7}$$

for the two isotope system and

$$L \propto \exp\left[\frac{\left(\delta^{18}O_p-\delta^{18}O_o\right)^2}{2\sigma^2_{\delta^{18}O}}\right]\cdot\exp\left[\frac{\left(\delta D_p-\delta D_o\right)^2}{2\sigma^2_{\delta D}}\right]\cdot\exp\left[\frac{\left(^{222}Rn_p-^{222}Rn_o\right)^2}{2\sigma^2_{^{222}Rn}}\right], \tag{8}$$

for the three isotope system. Here $\delta^{18}O_p$ and $\delta^{18}O_o$ are the predicted and observed measurements of $\delta^{18}O$, respectively, $\sigma_{\delta^{18}O}$ is the measurement uncertainty, and likewise for δD and ^{222}Rn.

Fractional contribution estimations from the application of the BMC model to a two isotope system ($\delta^{18}O$ and ^{222}Rn) are compared to the application of the BMC model to a three isotope system ($\delta^{18}O$, δD, and ^{222}Rn) in Figure 6a. The applications of the BMC model with different constraints show a systematic bias in the magnitude of contributions coming from each end-member source (Figure 6a); in particular, the contribution from surface snow is larger and more variable in the two isotope model than the three isotope model. This difference is likely due to the similarity of the snow and glacial melt samples in ^{222}Rn isotopic space (Figure 5). The additional isotope system (δD) separates the snow and glacial contributions in a third dimension. These data suggest that the inclusion of a third isotope increases the accuracy of the model. The introduction of a third isotope system as an additional constraint also increases the precision of the model; uncertainties are lower in all sample calculations for the three isotope model than the two isotope model (Figure 6b).

The estimated source fractional contributions from the model in this study, using $\delta^{18}O$, δD, and ^{222}Rn to calculate the relative contributions of the end-member sources, are within error of the linear mixing model utilized by *Bhatia et al.* [2011]. A direct comparison of the f_{ss}, f_g, and f_d estimations from our BMC model to the fractional contribution predictions from *Bhatia et al.* [2011], with both models utilizing the three isotope system ($\delta^{18}O$, δD, and ^{222}Rn), are found in Figure 7. The BMC model consistently produced f_{ss} estimations between 0.01 and 0.38, f_g estimations primarily between 0.4 and 0.95 (with a few lower fractional estimations between 0.17 and 0.26), and f_d estimations primarily between 0.07 and 0.37 (with a few estimations between 0.42 and 0.78). Thus, the fractional contributions resulting from our BMC model are in clear agreement with the fractional contributions predicted by *Bhatia et al.* [2011] (Figure 7). The *Bhatia et al.* [2011] model had no explicit calculations of uncertainties for the estimated fractional contributions; the BMC model takes the *Bhatia et al.* [2011] a step further by incorporating the uncertainties of the end-member isotopic compositions, which provides a range for the most likely fractional contributions from each end-member for each sample.

2.3. Case Study 3: Nutrient Sources to Hawaiian Soils Using ϵ_{Nd} and $^{87}Sr/^{86}Sr$

In addition to its applications for hydrological and glacial systems, this BMC model can also be applied to radiogenic isotopes as tracers. As an example we examine tropical soils in Hawaii using radiogenic isotopes ϵ_{Nd} and $^{87}Sr/^{86}Sr$ to assess the fractional contribution of bedrock, dust, and seaspray to this environment. Four depth transect soil samples from Long Substrate Age Gradient (LSAG) cores were analyzed for ϵ_{Nd} and

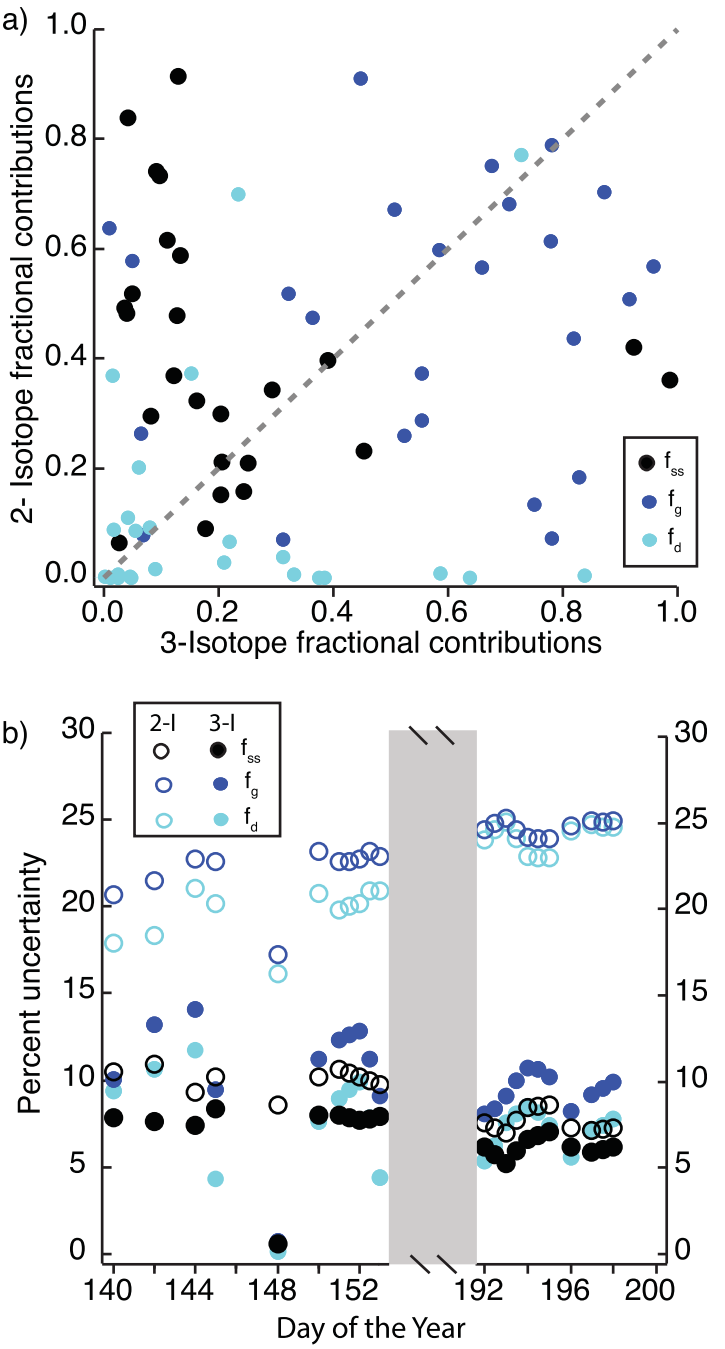

Figure 6. (a) Estimated fraction contributions f_{ss}, f_g, and f_d calculated from a two-isotope constrained model ($\delta^{18}O$ and ^{222}Rn) plotted against those calculated from a three-isotope model ($\delta^{18}O$, δD, and ^{222}Rn). Greenland Ice Sheet bulk water isotopic measurements taken from *Bhatia et al.* [2011]. Dashed gray line represents a 1:1 ratio of fractional contributions from the two isotope model and three isotope model. (b) Calculated uncertainties for the estimated fraction contributions from f_{ss}, f_g, and f_d. Open circles denote uncertainties from a model run using only two isotopes, $\delta^{18}O$ and ^{222}Rn (2-I). Filled circles denote uncertainties calculated from a model run using all three isotopes ($\delta^{18}O$, δD, and ^{222}Rn) (3-I).

$^{87}Sr/^{86}Sr$ and quartz abundance by *Kurtz et al.* [2001]. Relative contributions from the Asian dust end-member source were determined for these same samples in *Chadwick et al.* [1999] using a simple model that incorporated major cation measurements. The four cores analyzed by *Kurtz et al.* [2001] were collected from four locations in the Hawaiian Islands with distinct ages: Laupahoehoe, Big Island (20 ka), Kohala, Big Island (150 ka), Molokai (1400 ka), and Kauai (4100 ka).

Measurements of ϵ_{Nd} and $^{87}Sr/^{86}Sr$ provide isotopic fingerprints for sediment sourced from regions with contrasting lithologic and weathering histories. The three end-members for the isotope system used to describe these Hawaiian soil cores include Asian dust, Hawaiian basalt, and Pacific seawater. The ϵ_{Nd} and $^{87}Sr/^{86}Sr$ of surface Pacific seawater is known with confidence [*Tanaka et al.*, 2000]. The basalt and dust ϵ_{Nd} end-member values incorporated into the original model [*Chadwick et al.*, 1999] did not include uncertainties in the end-member compositions: to get more accurate fractional contribution estimates we have incorporated known uncertainties for the ϵ_{Nd} values of Hawaiian basalt [*Hanano et al.*, 2010] and Asian dust [*Biscaye et al.*, 1997]. Thus, we use the same end-member composition values as the original model but have also included a seawater ϵ_{Nd} value [*Tanaka et al.*, 2000; *Kennedy et al.*, 1998] and assess the relative errors of the estimations by incorporating uncertainties in the basalt and dust radiogenic compositions. The distinct isotopic compositions of each end-member enable the model to derive source fractional contributions at varying soil depths. End-member ε_{Nd} and $^{87}Sr/^{86}Sr$ values can be found in Table 3. The bulk composition soil ε_{Nd} and $^{87}Sr/^{86}Sr$ measurements are plotted with the source end-member ε_{Nd} and $^{87}Sr/^{86}Sr$ measurements in Figure 8.

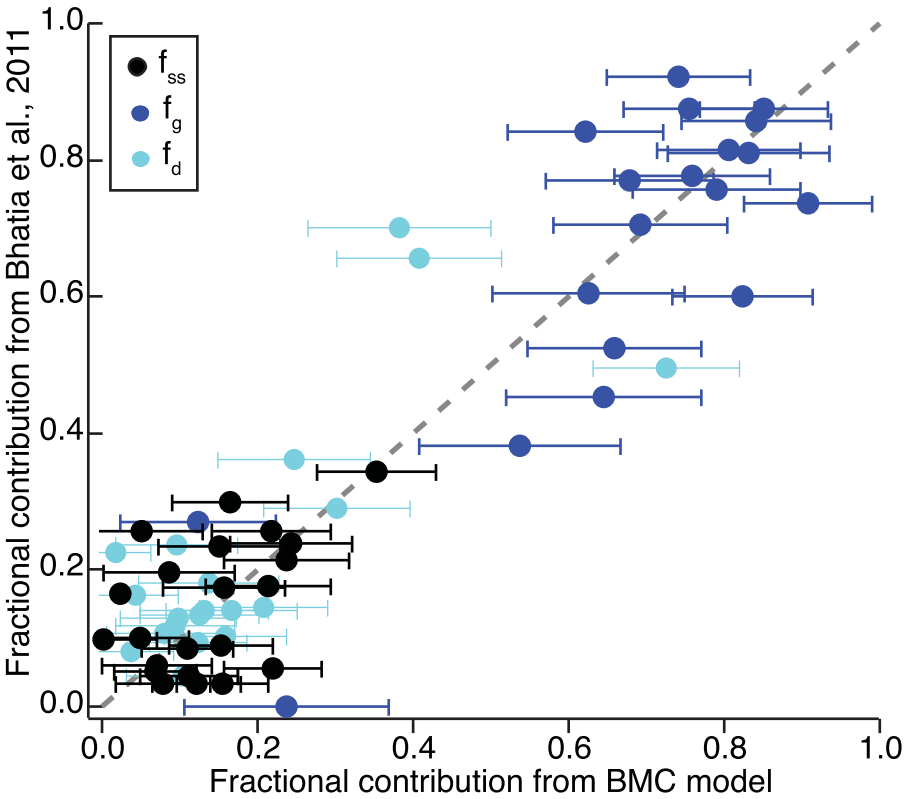

Figure 7. Comparison of fractional contributions for f_{ss}, f_g, and f_d calculated from $\delta^{18}O$, δD, and ^{222}Rn values of Greenland Ice Sheet bulk water samples by *Bhatia et al*. [2011] and the three isotope system Bayesian Monte Carlo mixing model from this study. The dashed gray line represents a 1:1 ratio of fractional contributions from model runs from *Bhatia et al*. [2011] and the BMC model. No error bars are available for the *y* axis, but *x* axis errors are the uncertainties produced in the BMC model.

2.3.1. Fractional Contribution to Hawaiian Soils

The fractional contributions of Asian dust to the Hawaiian soil core samples estimated by *Chadwick et al*. [1999] were determined using measurements of Th, Er, quartz, and Nd, and ranged between 0.01 and 0.87 fractional contribution estimations for all samples collected. *Chadwick et al*. [1999] did not break up the dust fractional contribution estimates based on location or depth, but rather combined all dust fractional contribution estimations into one plot. The original study investigated major cations compared to the age of the samples to find evidence that these end-member sources were present among all samples collected, but did not explicitly calculate Pacific seawater contributions. Our model was applied to the ε_{Nd} and $^{87}Sr/^{86}Sr$ measurements from the same Hawaiian soil core samples investigated in *Chadwick et al*. [1999] with the ε_{Nd} and $^{87}Sr/^{86}Sr$ of these samples published in *Kurtz et al*. [2001]. In this study, we estimate the fractional contribution of all three source end-members within each of the four sample locations independently, and compare the Asian dust fractional contributions calculated from our model to the ranges found in *Chadwick et al*. [1999].

In the application of our model to this case study, we assume that the Hawaiian soil samples have three possible contribution sources: Hawaiian basalt, Asian dust, and Pacific seawater. Thus, the sum of the fraction from basalt (f_b), fraction from dust (f_{du}), and fraction from seawater (f_{sw}) is constrained to equal 1

$$f_b + f_{du} + f_{sw} = 1. \tag{9}$$

The likelihood of a model prediction was calculated using

$$L \propto \exp\left[\frac{\left(\varepsilon\mathrm{Nd}_p - \varepsilon\mathrm{Nd}_o\right)^2}{2\sigma^2_{\varepsilon\mathrm{Nd}}}\right] \cdot \exp\left[\frac{\left(^{87}\mathrm{Sr}/^{86}\mathrm{Sr}_p - ^{87}\mathrm{Sr}/^{86}\mathrm{Sr}_o\right)^2}{2\sigma^2_{^{87}\mathrm{Sr}/^{86}\mathrm{Sr}}}\right], \tag{10}$$

where $\varepsilon\mathrm{Nd}_p$ and $\varepsilon\mathrm{Nd}_o$ are the predicted and observed measurements of ε_{Nd}, respectively, $\sigma_{\varepsilon\mathrm{Nd}}$ is the

Table 3. Isotopic End-Member Values From *Chadwick et al.* [1999] and *Tanaka et al.* [2000] (ϵ_{Nd} and $\sigma\epsilon_{Nd}$ of Pacific Seawater)[a]

End-Member	ϵ_{Nd}	$\sigma\epsilon_{Nd}$	$^{87}Sr/^{86}Sr$	$\sigma^{87}Sr/^{86}Sr$
Basalt	7	0.7	0.7035	0.0002
Dust	−10	1.2	0.7210	0.0035
Seawater	−9.6	0.9	0.7092	0.0001

[a]The $\sigma\epsilon_{Nd}$ values for Asian dust and Hawaiian basalt have been incorporated from previous publications [*Biscaye et al.*, 1997; *Hanano et al.*, 2010].

measurement uncertainty for $^{87}Sr/^{86}Sr$. The calculated soil source fractional contributions from our BMC model are presented in Figure 9. Estimated fractional contributions and uncertainties from the application of our model to the ε_{Nd} and $^{87}Sr/^{86}Sr$ measurements from these HI soil cores can be found in Table 3. The Laupahoehoe and Molokai soil depth transects followed similar trends with basalt as the dominant source contributor, consistently ranging from 0.60 to 0.97. Asian dust was the next largest contributor with a strong presence in the initial surface depths of 0.30–0.40, decreasing to fractional contributions of less than 0.15 as the depth of the transect increased. Pacific seawater composed the smallest source contributor, remaining less than 0.06 throughout both the Lapahoehoe and Molokai transects.

The Kohala core estimations produced the only fractional contribution trends in which the Asian dust was the dominant source contribution for the majority of the transect and where the Pacific seawater component was the strongest signal at the surface. Surface measurements indicated a basalt fractional contribution of 0.34, a dust fractional contribution of 0.02, and a high seawater contribution of 0.64. With increasing depth, the Pacific seawater component became the smallest source contributor remaining at fractional contribution values of less than 0.04 throughout the rest of the transect. With increasing depth, the Asian dust component became the dominant source contributor throughout the middle depths of the transect with fractional contribution values of 0.61–0.94 before decreasing to 0.18 at 60 cm depth. The basalt component initially decreased with depth, with fractional contribution values of less than 0.06 for the middle segment of the transect before increasing with depth to become the dominant fractional contribution of 0.81 at 60 cm depth.

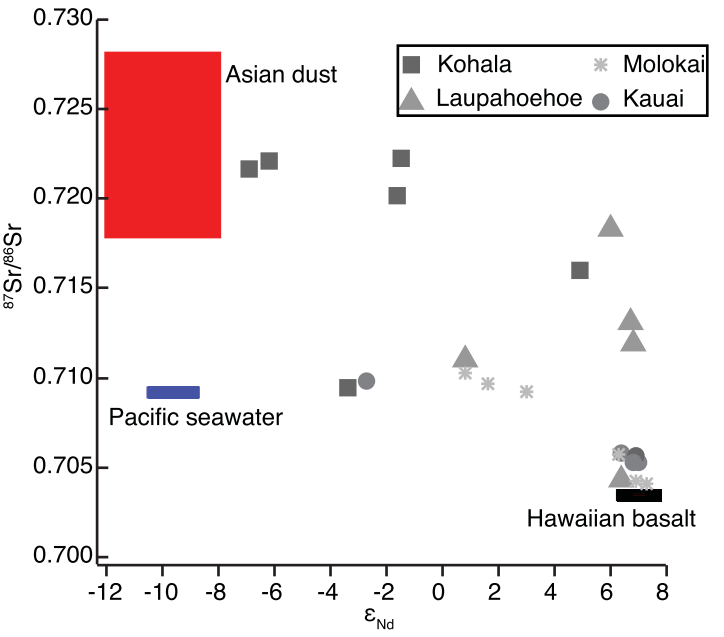

Figure 8. Dual isotope plot of ϵ_{Nd} and $^{87}Sr/^{86}Sr$ values of Hawaiian soil samples taken from *Chadwick et al.* [1999] and *Kurtz et al.* [2001]. Rectangles represent the mean isotopic end-member values and variation in end-member values for Hawaiian basalt, Asian dust, and Pacific seawater, measurements taken from *Chadwick et al.* [1999], *Kurtz et al.* [2001], and *Tanaka et al.* [2000]. End-member isotopic compositions and uncertainties can be found in Table 3.

The Kauai core estimations placed the basalt and seawater components at roughly equal fractional contributions at the surface of 0.41. With increasing depth, the seawater component decreased to fractional contribution values of less than 0.07 while the basalt component increased to fractional contribution values of more than 0.9 for the remaining depth of the transect. The dust component in the Kauai core composed a fractional contribution of 0.18 at the surface and remained between values of 0.05 and 0.09 through the final depth measured. A potential reason that the Kohala and Kauia samples display notable amounts of Pacific seawater contributions near the surface

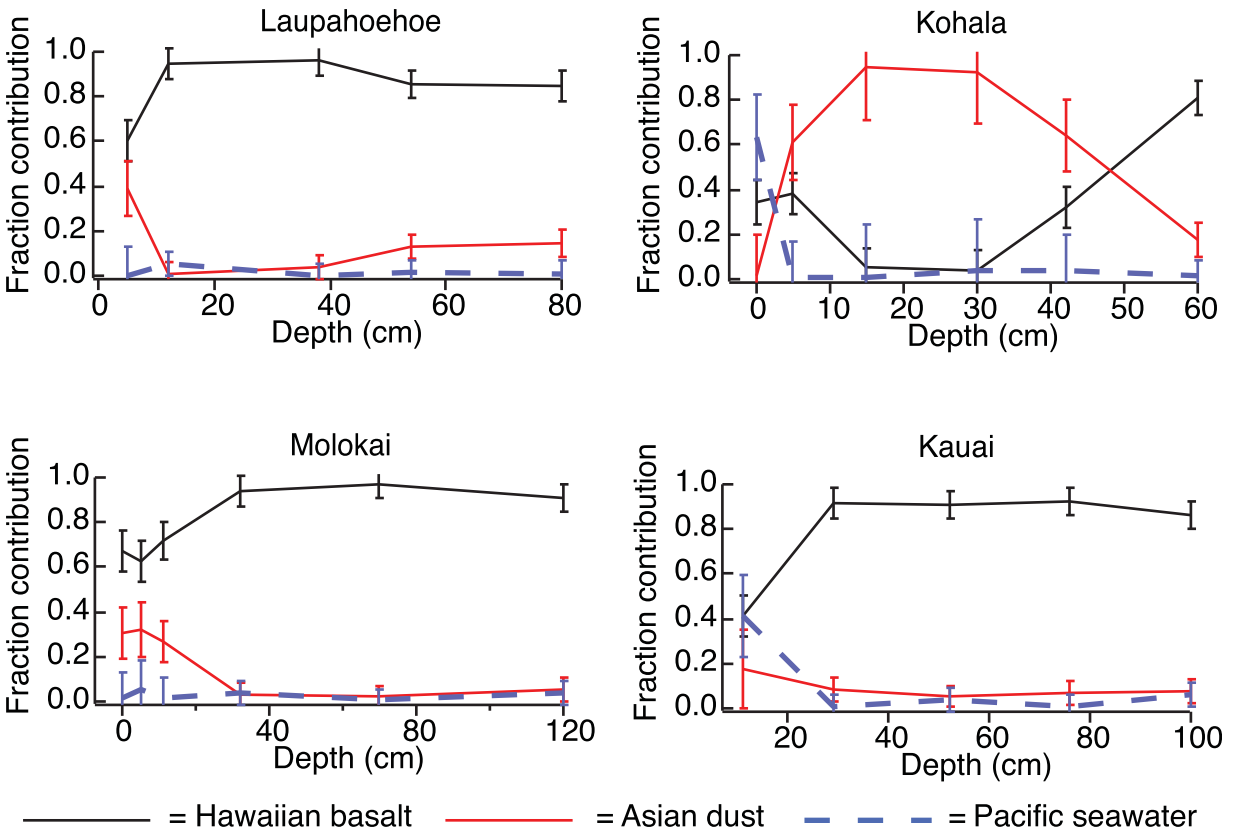

Figure 9. Fractional contributions, f_b, f_{du}, and f_{sw}, to Hawaiian soil transects using the BMC model, end-member compositions as indicated in Figure 8, and ϵ_{Nd} and $^{87}Sr/^{86}Sr$ measurements of samples described in *Chadwick et al.* [1999] and *Kurtz et al.* [2001].

is that these two locations are situated in the northwest of their respective islands, which corresponds to the wind trajectory and may be cause for an elevated seawater component.

Even with error bars (encompassing all uncertainties in these Hawaiian soil fractional contribution estimations of Hawaiian basalt, Asian dust, and Pacific seawater) the transect fractional contribution trends are distinct between sources and locations (Figure 9). The estimated Asian dust fractional contributions from the model in this study, using only ε_{Nd} and $^{87}Sr/^{86}Sr$ to calculate the relative contributions of the end-member sources, are within error of the original Asian dust fractional contribution estimations from the mixing model utilized in *Chadwick et al.* [1999]. The BMC implementation provides two additions: (1) a calculation of the fractional contribution of seaspray to the soil budget and (2) uncertainty in the calculated fractions.

3. Model Limitations

In assuming that the bulk samples are derived from only three possible sources in all three case studies, we limit the complexity of the system. Possible sources of error in our BMC model may arise from our assumption that the end-member values do not covary, as compared to end-members in *Cable et al.* [2011]. We observed no physical evidence to suggest a covariance between isotopic compositions from the three different melt sources at the Athabasca Glacier, and the original GrIS melt and Hawaiian soil publications did not indicate the existence of such processes. Thus, we chose not to represent such relationships in our case studies.

For the Athabasca Glacier and GrIS case studies, the end-member uncertainties do not incorporate temporal changes in end-member values. Specifically, in the case of the GrIS case study, ^{222}Rn values

for delayed flow waters likely exhibit temporal variations, due to variations in the residence time of subglacial water (C. A. Arendt et al., submitted manuscript, 2015) that are not accounted for in the initial model. The division of the delayed flow end-member into two separate end-members (fast-flow and slow-flow) would place constraints on variations in ^{222}Rn values that originated from temporal disparities and provide a more detailed quantification of relative contributions. A potential additional uncertainty constraint that could be incorporated into both the Athabasca Glacier and GrIS case studies would be to utilize the deuterium excess.

Using the linear multicomponent Bayesian Monte Carlo mixing model presented in this study, estimations of fractional contributions from sources are more precise if end-member compositions are distinct from one another. In analyzing the end-member compositions from the Greenland Ice Sheet case study (Figure 5), it is apparent that the surface snow, glacial ice, and delayed flow water isotopic compositions overlap with one another. This overlap is likely the main source of uncertainty observed in our fractional contribution estimates (Figure 7). The uncertainties associated with the estimated fractional contributions decrease with the degree to which the end-member isotopic compositions are distinguishable from one another. The end-member isotopic compositions for the Athabasca Glacier and Hawaiian soil case studies are notably distinct (Tables 1 and 3 and Figures 2 and 8), causing the degree of uncertainty in the fractional contribution estimates to be low (Figures 3 and 9).

4. Broader Implications

The multicomponent linear BMC mixing model presented in this study is shown to be widely applicable to numerous Earth surface systems and can be extended to systems beyond soil nutrients and melt contributions in glacial environments (i.e., dust provenance records, water mass mixing, and ecological systems). The model is capable of accounting for both prior information and assumptions of a given system. This open source linear isotopic mixing BMC model is applicable to many environments because it allows for the addition of end-members, further constraints and isotopic systems, and the incorporation of large uncertainties in end-member values. End-member isotopic compositions can encapsulate both spatial and temporal variation in their assigned standard deviation values, which can be critical in certain types of case studies (i.e., alpine glacier, time series samples, etc.). Furthermore, understanding how well these estimated fractional contribution values are known (estimation of uncertainty) allows for a more complete representation of a system. Because the coding for this multicomponent linear BMC mixing model is supplied in the supporting information, it can be readily adapted to both new and existing data sets to infer source contributions in Earth surface systems.

5. Conclusions

This study has validated the relevance and applicability of our linear multicomponent BMC mixing model to derive contribution fractions in Earth surface systems with source end-members that have distinct isotopic signatures. The application of our model to a new data set from the Athabasca Glacier resulted in statistically significant fractional contribution estimates that followed expected seasonal trends for alpine glacier melt evolution [*Cable et al.*, 2011; *Hindshaw et al.*, 2011]. The application of our model to two additional case studies in differing locations using diverse isotope systems resulted in fractional contributions comparable to those calculated in their initial publications [*Kennedy et al.*, 1998; *Chadwick et al.*, 1999; *Kurtz et al.*, 2001; *Chadwick et al.*, 2009; *Bhatia et al.*, 2011]. The addition of a third isotopic system in the Greenland Ice Sheet case study resulted in decreased uncertainty of the fractional contribution estimations by placing additional constraints on the most likely fractional contributions that are unaccounted for in a two isotope system. The Matlab script presented here is straightforward for users to modify the priors of the end-member isotopic compositions. For instance, inclusions of different analytic or empirical PDFs, correlations in compositions, or more complex variability in the isotopic compositions can be modified into the script. However, these modifications should be done on a case-by-case basis based on physical observations of the Earth surface system of interest. Thus, the BMC estimation strategy supplied here can be used to effectively generate solutions and associated uncertainties for mass partitioning of distinct input end-members from bulk samples in a variety of Earth surface systems and is easily accessible to a diverse range of scientific applications.

Acknowledgments
This research was funded by the University of Michigan Rackham Graduate School and the Turner Award from the Department of Earth and Environmental Sciences to C.A.A. We would like to thank Sarah Aarons for her assistance in the collection of samples used for the Athabasca Glacier case study. Data sets supporting this manuscript are available in supporting information Tables S1 and S2. We would also like to thank Sarah Das, Maya Bhatia, and Oliver Chadwick for their cooperation and assistance in obtaining the isotopic values and fractional contribution estimations from the original studies of the data used in case studies 2 and 3.

References

Aizen, V. B., E. M. Aizen, K. Fujita, S. A. Nikitin, K. J. Kreutz, and L. N. Takeuchi (2005), Stable-isotope time series and precipitation origin from firn-core and snow samples, Altai glaciers, Siberia, *J. Glaciol.*, *51*(175), 637–654.

Barber, R. W., and M. J. Wearing (2001), A mathematical model for estimating the pollution exchange coefficient of small tidal embayments, in *Water Resource Management*, vol. 4, edited by C. A. Brebbia, pp. 331–340, WIT Press, Southampton, U. K.

Barnett, T. P., J. C. Adam, and D. P. Lettenmaier (2005), Potential impacts of a warming climate on water availability in snow-dominated regions, *Nature*, *438*(7066), 303–309, doi:10.1038/nature04141.

Bhatia, M. P., S. B. Das, E. B. Kujawinski, P. Henderson, A. Burke, and M. A. Charette (2011), Seasonal evolution of water contributions to discharge from a Greenland outlet glacier: Insight from a new isotope-mixing model, *J. Glaciol.*, *57*(205), doi:10.3189/002214311798043861.

Biscaye, P. E., F. E. Grousset, M. Revel, S. Van der Gaast, G. A. Zielinski, A. Vaars and G. Kukla (1997), Asian provenance of glacial dust (stage 2) in the Greenland Ice Sheet Project 2 Ice Core, Summit, Greenland, *J. Geophys. Res.*, *102*(C12), 26,765–26,781, doi:10.1029/97JC01249.

Brugmann, M. N., and M. M. Demuth (1994), Surface and basal topography of the Athabasca Glacier: A glaciological interpretation and recommendation for the location of near-ice interpretive facilities, contract report, Jasper Natl. Park, pp. 190–193, Natl. Hydrol. Res. Inst., Saskatoon, Saskatchewan, Canada.

Butler, D. (1980), Shallow core snow chemistry of Athabasca Glacier, Alberta, *J. Earth Sci.*, *17*, 278–281, doi:10.1139/e80-024.

Cable, J., K. Ogle, and D. Williams (2011), Contribution of glacier meltwater to streamflow in the Wind River Range, Wyoming, inferred via a Bayesian mixing model applied to isotopic measurements, *Hydrol. Processes*, *25*(14), 2228–2236, doi:10.1002/hyp.7982.

Canada National Climate Archive (2013), National climate data and information archive, technical report no. Alberta 5, 2011-7, 2011, Natl. Clim. Data Cent., Fredericton, New Brunswick, Canada.

Chadwick, O. A., L. A. Derry, P. M. Vitousek, B. J. Huebert, and L. O. Hedin (1999), Changing sources of nutrients during four million years of ecosystem development, *Nature*, *397*, 491–497, doi:10.1038/17276.

Chadwick, O. A., L. A. Derry, C. R. Bern, and P. M. Vitousek (2009), Changing sources of strontium to soils and ecosystems across the Hawaiian Islands, *Chem. Geol.*, *267*, 64–76, doi:10.1016/j.chemgeo.2009.01.009.

Clark, I., and P. Fritz (1997), *Environmental Isotopes in Hydrogeology*, pp. 1–331, CRC Press, Boca Raton, Fla.

Cooper, L. W. (1998), Isotope Tracers in Catchment Hydrology, Isotope fractionation in snowcover, chap. 4, edited by C. Kendall and J. J. McDonnell, 119–136, Elsevier Sci., Amsterdam, Netherlands.

Craig, H. (1961), Isotopic variations in meteoric waters, *Science*, *133*(3465), 1702–1703, doi:10.1126/science.133.3465.1702.

Dansgaard, W. (1964), Stable isotopes in precipitation, *Tellus*, *16*(4), 436–468, doi:10.1111/j.2153-3490.1964.tb00181.x.

Falcone, M. D. (2007), Assessing hydrological processes controlling the water balance of lakes in the Peace-Athabasca Delta, Alberta, Canada using water isotope tracers, PhD thesis, Univ. of Waterloo, Ont., Canada.

Ford, D. C., P. L. Smart and R. O. Ewers (1983), The physiography and speleogenesis of Castleguard Cave, Columbia Icefields, Alberta, Canada, *Arct. Alp. Res.*, *15*(4), 437–450, doi:10.2307/1551231.

Fortner, S. K., W. B. Lyons, A. G. Fountain, K. A. Welch, and N. M. Kehrwald (2009), Trace element and major ion concentrations and dynamics in glacier snow and melt: Eliot Glacier, Oregon Cascades, *Hydrol. Processes*, *23*, 2987–2996, doi:10.1002/hyp.7418.

Gat, J. R. (1996), Oxygen and hydrogen isotopes in the hydrologic cycle, *Annu. Rev. Earth Planet. Sci.*, *24*(1), 225–262, doi:10.1146/annurev.earth.24.1.225.

Grupe, G. (2014), Application of isotopic mixing models for palaeodietary and paleoecological studies, *Anthropol. Anzeiger*, *71*, 21–39, doi:10.1127/0003-5548/2014/0375.

Hanano, D. W., D. Weis, J. S. Scoates, S. Aciego and D. J. DePaolo (2010), Horizontal and vertical zoning of heterogeneities in the Hawaiian mantle plume from the geochemistry of consecutive postshield volcano pairs: Kohala-Mahukona and Mauna Kea–Hualalai, *Geochem. Geophys. Geosyst.*, *11*, Q01004, doi:10.1029/2009GC002782.

Hart, J. K. (2006), Athabasca Glacier, Canada—A field example of subglacial ice and till erosion?, *Earth Surf. Processes Landforms*, *31*, 65–80, doi:10.1002/esp.1233.

Hindshaw, R. S., E. T. Tipper, B. C. Reynolds, E. Lemarchand, J. G. Wiederhold, J. Magnusson, S. M. Bernasconi, R. Kretzschmar, and B. Bourdon (2011), Hydrological control of stream water chemistry in a glacial catchment (Damma Glacier, Switzerland), *Chem. Geol.*, *285*, 215–230, doi:10.1016/j.chemgeo.2011.04.012.

Hooper, R. P., and C. A. Shoemaker (1986), A comparison of chemical and isotopic hydrograph separation, *Water Resour. Res.*, *22*(10), 1444–1454, doi:10.1029/WR022i010p01444.

Hubbard, B. P., M. J. Sharp, I. C. Willis, M. K. Nielsen, and C. C. Smart (1995), Borehole waterlevel variations and the structure of the subglacial hydrological system of Haut Glacier d'Arolla, Valais, Switzerland, *J. Glaciol.*, *41*, 572–583.

Kehrwald, N. M., L. G. Thompson, Y. Tandong, E. Mosley-Thompson, U. Schotterer, V. Alfimov, J. Beer, J. Eikenberg and M. E. Davis (2008), Mass loss on Himalayan glacier endangers water resources, *Geophys. Res. Lett.*, *35*, L22503, doi:10.1029/2008GL035556.

Kennedy, M. J., O. A. Chadwick, P. M. Vitousek, L. A. Derry, and D. M. Hendricks (1998), Changing sources of base cations during ecosystem development, Hawaiian Islands, *Geology*, *26*(11), 1015–1018, doi:10.1130/0091-7613(1998)026¡1015:CSOBCD¿2.3.CO;2.

Kurtz, A. C., L. A. Derry, and O. A Chadwick (2001), Accretion of Asian dust to Hawaiian soils: Isotopic, elemental, and mineral mass balances, *Geochim. Cosmochim. Acta*, *65*(12), 1971–1983, doi:10.1016/S0016-7037(01)00575-0.

Letreguilly, A. (1988), Relation between the mass balance of western Canadian mountain glaciers and meteorological data, *J. Glaciol.*, *34*(116), 11–18, doi:10.1029/2007GL030780.

Liu, F. J., R. C. Bales, M. H. Conklin and M. E. Conrad (2008), Streamflow generation from snowmelt in semi-arid, seasonally snow-covered, forested catchments, Valles Caldera, New Mexico, *Water Resour. Res.*, *44*, W12443, doi:10.1029/2007WR006728.

McCluney, K. E., and J. L. Sabo (2010), Tracing water sources of terrestrial animal populations with stable isotopes: Laboratory tests with crickets and spiders, *Plos One*, *5*(12), e15696, doi:10.1371/journal.pone.0015696.

Moore, J. W., and B. X. Semmens (2008), Incorporating uncertainty and prior information into stable isotope mixing models, *Ecol. Lett.*, *11*(5), 470–480, doi:10.1111/j.1461-0248.2008.01163.x.

Morlock, S. E., H. T. Nguyen, and J. H. Ross (2002), Feasibility of acoustic Doppler velocity meters for the production of discharge records from U.S. Geological Survey streamflow-gaging stations, *Water Resour. Invest. Rep., 01–4157*, 1–56.

Mosegaard, K., and A. Tarantola (1995), Monte Carlo sampling of solutions to inverse problems, *J. Geophys. Res.*, *100*(B7), 12,431–12,447, doi:10.1029/94JB03097.

Ogle, K., R. L. Wolpert, and J. F. Reynolds (2004), Reconstructing plant root area and water uptake profiles, *Ecology*, *85*(7), 1967–1978, doi:10.1890/03-0346.

Parnell, A., D. Phillips, S. Bearhop, B. Semmens, E. Ward, J. Moore, A. Jackson, J. Grey, D. Kelly, and R. Inger (2013), Bayesian stable isotope mixing models, *Environmetrics*, *24*(6), 387–399, doi:10.1002/env.2221.

Parnell, A. C., R. Inger, S. Bearhop, and A. L. Jackson (2010), Source partitioning using stable isotopes: Coping with too much variation, *Plos One*, *5*(3), e9672, doi:10.1371/journal.pone.0009672.

Petit, J. R., et al. (1999), Climate and atmospheric history of the past 420,000 years from the Vostok ice core, Antarctica, *Nature*, *399*, 429–436, doi:10.1038/20859.

Pichler, T. (2005), Stable and radiogenic isotopes as tracers for the origin, mixing, and subsurface history of fluids in submarine shallow-water hydrothermal systems, *J. Volcanol. Geotherm. Res.*, *139*(3–4), 211–226, doi:10.1016/j.jvolgeores.2004.08.007.

Rickli, J., M. Frank, A. R. Baker, S. Aciego, G. de Souza, R. B. Georg, and A. N. Halliday (2010), Hafnium and neodymium isotopes in surface waters of the eastern Atlantic Ocean: Implications for sources and inputs of trace metals to the ocean, *Geochim. Cosmochim. Acta*, *74*, 540–557, doi:10.1016/j.gca.2009.10.006.

Sharp, M., G. H. Brown, M. Tranter, I. C. Willis, and B. Hubbard (1995), Comments on the use of chemically based mixing models in glacier hydrology, *J. Glaciol.*, *41*(138), 241–246.

Shea, J. M., and S. J. Marshall (2007), Atmospheric flow indices, regional climate, and glacier mass balance in the Canadian Rocky Mountains, *Int. J. Climatol.*, *27*(2), 233–247, doi:10.1002/joc.1398.

Singh, B. P. (2013), Isotopic composition of water in precipitation in a region or place, *Appl. Radiat. Isot.*, *75*, 22–25, doi:10.1016/j.apradiso.2013.01.013.

Singh, P., and L. Bengtsson (2005), Impact of warmer climate on melt and evaporation for the rainfed, snowfed and glacierfed basins in the Himalayan region, *J. Hydrol.*, *300*(1–4), 140–154, doi:10.1016/j.jhydrol.2004.06.005.

Smart, C. C. (1983), The hydrology of Castleguard Karst, Columbia Icefields, Alberta, Canada, *Arct. Alp. Res.*, *15*(4), 471–486.

Socki, R. A., H. R. Karlsson, and E. K. Gibson Jr. (1992), Extraction technique for the determination of O-18 in water using preevacuated glass vials, *Anal. Chem.*, *64*(7), 829–831, doi:10.1021/ac00031a026.

Souchez, R. (1984), On the isotopic composition in delta-D and delta-O-18 of water and ice during freezing, *J. Glaciol.*, *30*(106), 369–372.

Souchez, R. (2000), Basal ice formation and deformation in central Greenland: A review of existing and new ice core data, *Geol. Soc. Spec. Publ.*, *176*(0305–8719), 13–22, doi:10.1144/GSL.SP.2000.176.01.02.

Souchez, R., M. Lemmens, J.-L. Tison, R. Lorrain, and L. Janssens (1983), Reconstruction of basal boundary conditions at the Greenland Ice Sheet margin from gas composition in the ice, *Earth Planet. Sci. Lett.*, *118*(1–4), 327–333, doi:10.1016/0012-821X(93)90176-A.

Soulsby, C., J. Petry, M. J. Brewer, S. M. Dunn, B. Ott, and I. A. Malcolm (2003), Identifying and assessing uncertainty in hydrological pathways: A novel approach to end member mixing in a Scottish agricultural catchment, *J. Hydrol.*, *274*(1–4), 109–128, doi:10.1016/S0022-1694(02)00398-0.

Stewart, I. T. (2009), Changes in snowpack and snowmelt runoff for key mountain regions, *Hydrol. Processes*, *23*(1), 78–94, doi:10.1002/hyp.7128.

Tanaka, T., et al. (2000), JNdi-1: A neodymium isotopic reference in consistency with LaJolla neodymium, *Chem. Geol.*, *168*, 279–281, doi:10.1016/S0009-2541(00)00198-4.

Taylor, S., X. Feng, J. W. Kirchner, R. Osterhuber, B. Klaue, and C. E. Renshaw (2001), Isotopic evolution of a seasonal snowpack and its melt, *Water Resour. Res.*, *37*(3), 759–769, doi:10.1029/2000WR900341.

Thayyen, R. J., J. T. Gergan, and D. P. Dobhal (2007), Role of glaciers and snow cover on headwater river hydrology in monsoon regime—Micro-scale study of Din Gad catchment, Garhwal Himalaya, India, *Curr. Sci.*, *92*(3), 376–382.

Theakstone, W. H. (2003), Oxygen isotopes in glacier-river water, Austre Okstindbreen, Norway, MS thesis, Univ. of Manchester, Manchester, U. K.

Unnikrishna, P. (2002), Isotope variations in a Sierra Nevada snowpack and their relation to meltwater, *J. Hydrol.*, *260*, 38–57, doi:10.1016/S0022-1694(01)00596-0.

Verbunt, M., J. Gurtz, K. Jasper, H. Lang, P. Warmerdam, and M. Zappa (2003), The hydrological role of snow and glaciers in alpine river basins and their distributed modeling, *J. Hydrol.*, *282*(1–4), 36–55, doi:10.1016/S0022-1694(03)00251-8.

Wikle, C. K. (2003), Hierarchical models in environmental science, *Int. Stat. Rev.*, *71*(2), 181–199, doi:10.1111/j.1751-5823.2003.tb00192.x.